Electronic Supplementary Material (ESI) for Lab on a Chip.

Supplementary Information

A Portable Smart Phone Based Plasmonic Nanosensor Readout Platform that Measures Transmitted Light Intensities of Nanosubstrates Using an Ambient Light Sensor

Q. Fu[a,1], Z. Wu[a,1], F. Xu[b], X. Li[a], C. Yao[a], X. Meng[c], L. Sheng[c], S. Yu[a], Y. Tang[a, d] *

[a] Department of Bioengineering, Guangdong Province Key Laboratory of Molecular Immunology and Antibody Engineering, Jinan University, Guangzhou 510632, PR China.

[b] School of Software Engineering, HuaZhong University Of Science and Technology, Wuhan, 430074, PR China.

[c] Oncology Department of the first affiliated hospital of Jinan University, Guangzhou 510632, PR China.

[d] Institute of Biotranslational Medicine, Jinan University, Guangzhou, 510632, PR China

*Corresponding authors: Fax: (+86)-20-85227003; Tel: (+86)-20-85227003; E-mail: ty-jaq7926@163.com.

[1] These authors contributed equally to the manuscript.

Results

1. Corresponding relationship of measured results from smart phone based PNRP and commercial UV-vis spectroscopy

In order to study the corresponding relationship of measured results from PNRP and commercial UV-vis spectroscopy, triangular AgNPRs was concentrated or diluted different ploids, and then their transmitted light intensities and absorbance were measured by PNRP and commercial UV-vis spectroscopy. As measured absorbance from commercial microplate reader increased, transmitted light intensity measured by the smart phone based plasmonic nanosensors reader decreased.

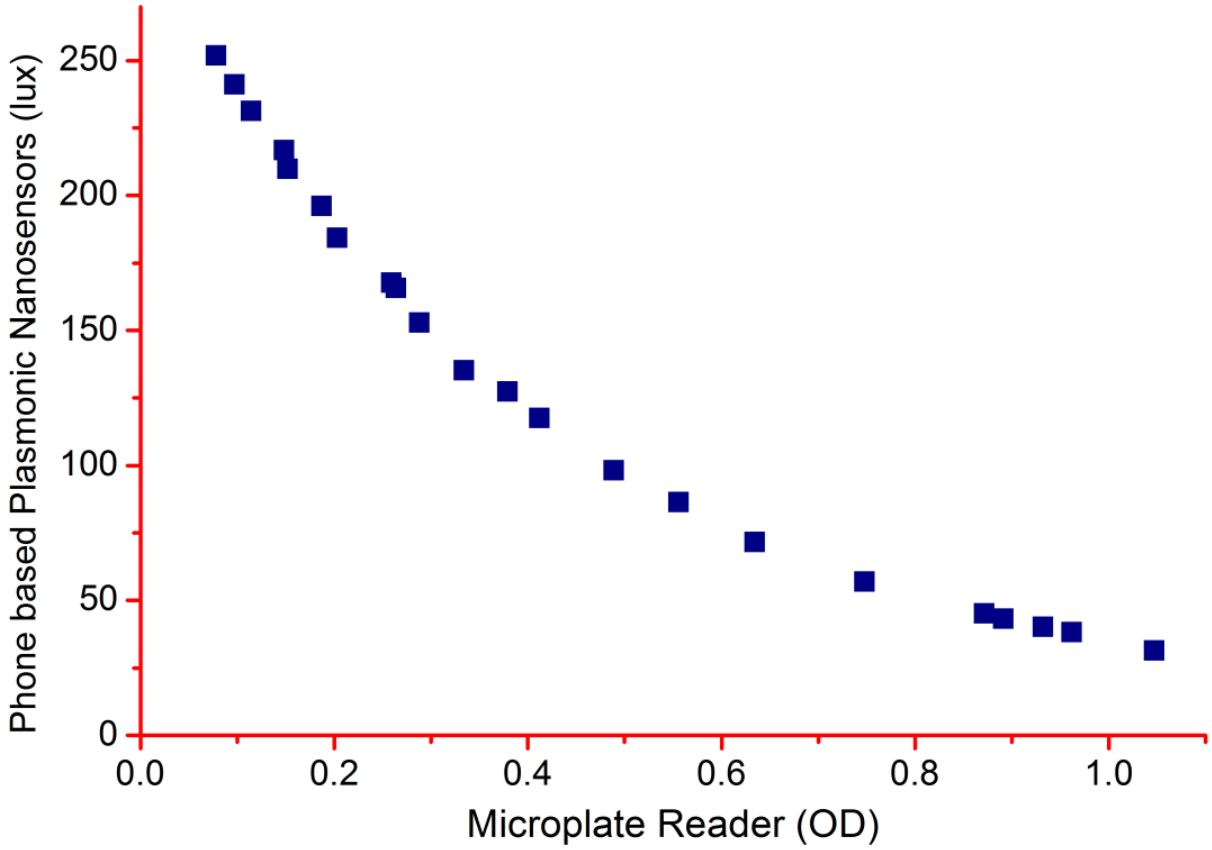

Figure S1. Accuracy of the smart phone based PNRP. As measured absorbance from commercial microplate reader increased, transmitted light intensity measured by the smart phone based plasmonic nanosensors reader index decreased.

2. Stability of this smart phone based PNRP

The purpose of this experiment was to study the stability of the smart phone-based PNRP. Using the PNRP, we performed ten replicate measurements of the transmitted light intensities of different concentrations of triangular AgNPRs. These ten measurements were taken separately. After each measurement, the software was stopped, and for thenext measurement, the software was restarted before measuring the transmitted light intensity. The time interval of each measurement was approximately 1 min.

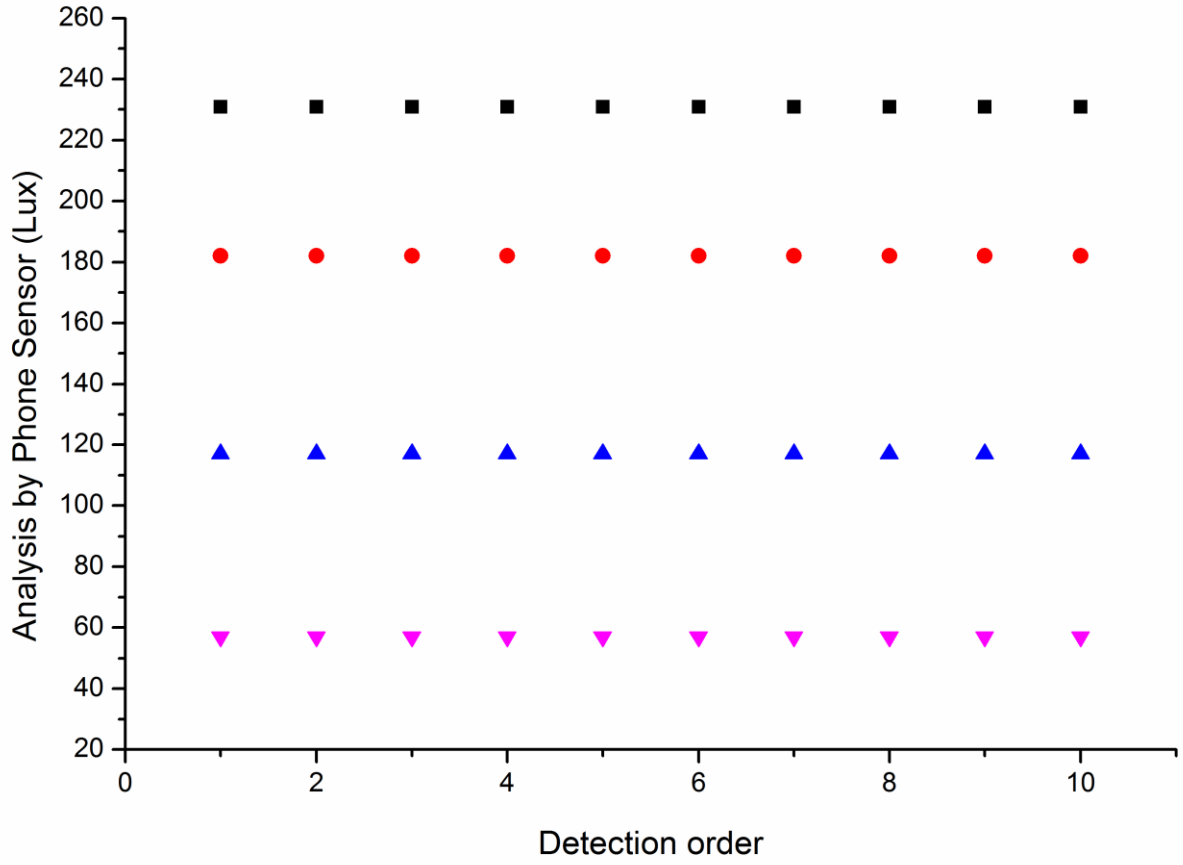

Figure S2. Stability of this smart phone based PNRP. Transmitted light intensities of different concentrations triangular AgNPRs were measured with 10 duplicates. Results showed that each measurement was identical, proving the smart phone based PNRPs stability.

3. Universality of the smart phone based NPRP running on different smart phones

We researching the universality of the smart phone based NPRP for different brands of smart phones. Six brands of smart phones were used to measure ambient light intensity under the same conditions and yielded identical results, indicating that the development of the smart phone based NPRP was applicable for different brands of smart phones.

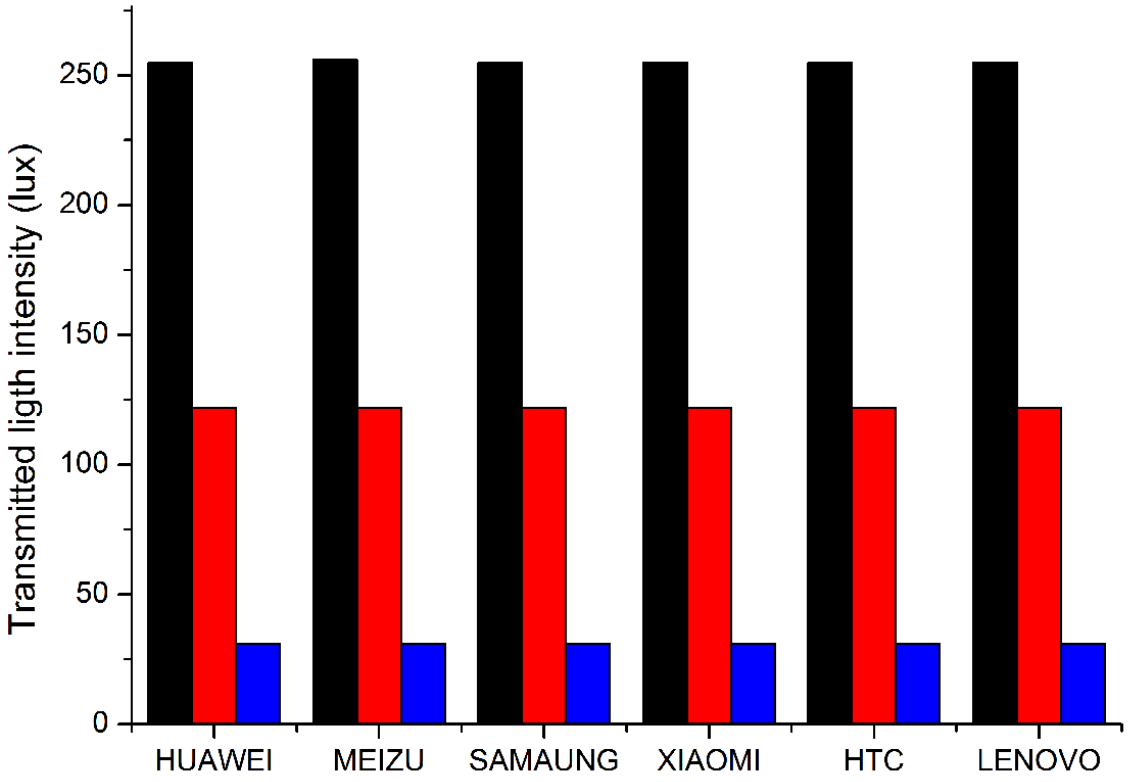

Figure S3. Universality of the smart phone based NPRP for different brands of smart phones. We researching the universality of the smart phone based NPRP for different brands of smart phones. Under the same conditions, light intensities of 6 brands of smart phones' measurements were the same. There indicated that the development of the smart phone based NPRP was applicable for different brands of smart phones.

4. Duration time of the smart phone based NPRP's battery

To study duration time of smart phone based NPRP's battery, transmitted light intensities of different concentrations triangular AgNPRs was measure by the smart phone based NPRP. In the process of measurement, switch of the smart phone based NPRP open 5 min and then keep closed 5 min,and this process in turn again. When the switch is open, light intensities of triangular AgNPRs were measured and recorded every minute. Our results shown that measured transmitted light intensities of smart phone based NPRP measured were equal during a period of 140 minutes. After 140 min, measurement results were fluctuates and decrease. Considering every measurement of plasmonic nanosensors was taken 3 s, causing us to believe that the smart phone based NPRP's battery could be used repeatedly for 2,800 times.

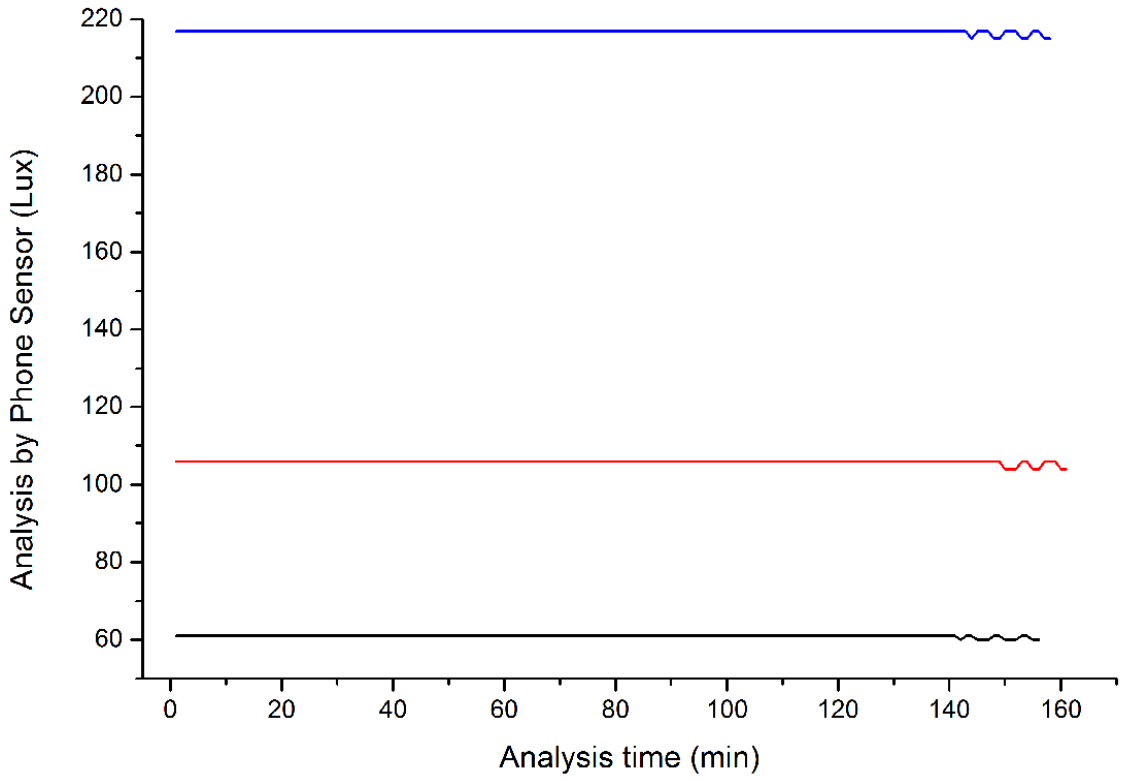

Figure S4. Duration time of the smart phone based NPRP's battery. We turned its switch on and off in 5 minute intervals to measure light intensity. Our results shown that transmitted light intensity of smart phone based NPRP measured were consistent during a period of 140 minutes. Every measurement of plasmonic nanosensors was taken three seconds, causing us to believe that the smart phone based NPRP's battery could be used repeatedly for 2,800 times.

5. Hydrogen peroxide adjusts LSPR of triangular AgNPRs

Hydrogen peroxide is a powerful oxidizing agent. To optimize the concentrations of H_2O_2 used to etch triangular AgNPRs, 100 µL AgNPRs were mixed with 100 µL different concentrations of H_2O_2 (0 - 90 µM). After 30 min, LSPR and transmitted light intensity were measured. As shown in figure S 5a, as the concentrations of H_2O_2 increase, the LSPR peaks show a gradual blue shift and absorbance at 680 nm decrease, as well as transmitted light intensity of AgNPRs increase (figure S5b). The absorbance and transmitted light intensity are highly associated with the concentrations of H_2O_2. When the H_2O_2 concentrations are greater than 80 µM, the differences in degrees of absorbance and transmitted light intensities are reduced. Therefore, in our experiment, we have chosen the H_2O_2 concentration as 80 µM in following experiments.

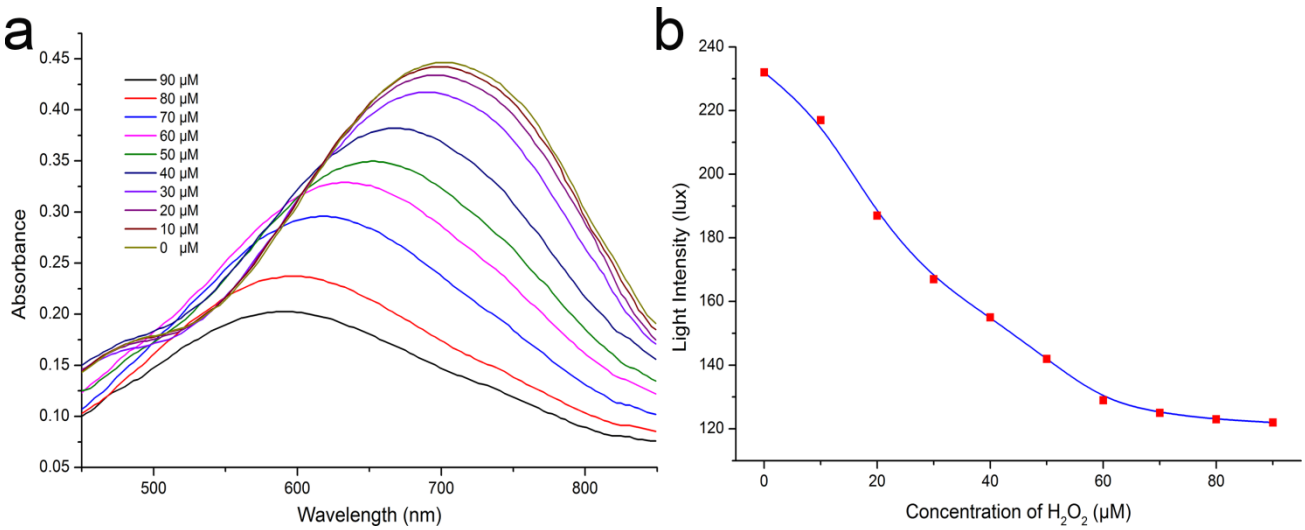

Figure S 5. Hydrogen peroxide adjusts LSPR of triangular AgNPRs. When the H_2O_2 concentrations are greater than 80 µM, the differences in degrees of the absorbance and transmitted light intensities are reduced. Therefore, in our experiment, we have chose the H_2O_2 concentration as 80 µM.

6. Au@PtNPs adjusts LSPR of triangular AgNPRs

To ensure sensitivity of the assay, we first needed to find an efficient and stable catalyst to decompose H_2O_2. In our research, core-shelled Au@Pt nanoparticles (Au@PtNPs) were chosen because they proved to be very efficient and stable catalysts for decomposition of H_2O_2. Au@PtNPs were labeled with anti-CEA mAb and then blocked by sealers. Different concentrations of mAb-Au@PtNPs were mixed with 80 μM H_2O_2 to catalyze its decomposition. After 30 min, 100 μL triangular AgNPRs were concentrated twice and then mixed with these solutions. After 30 min, LSPR absorbance and transmitted light intensity were measured. As shown in figure S6, as the concentrations of mAb-Au@PtNPs decrease, the LSPR peaks of AgNPRs show a gradual blue shift and absorbance intensity at 680 nm decrease, as well as transmitted light intensity of AgNPRs increase. Measured LSPR absorbance and transmitted light intensity are highly associated concentrations of mAb-Au@PtNPs. When concentration of mAb-Au@PtNPs, it can decomposed H_2O_2 obviously, indicating mAb-Au@PtNPs is an efficient and stable catalyst in our research.

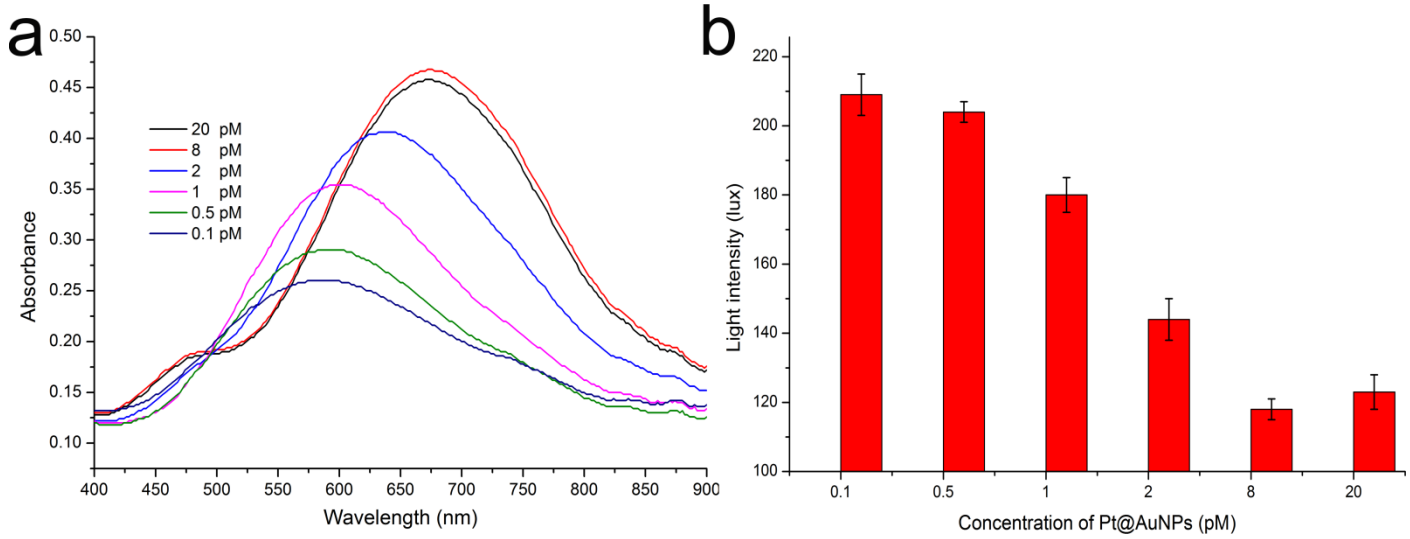

Figure S6. Au@PtNPs adjusts LSPR of triangular AgNPRs. The measured LSPR absorbance and transmitted light intensity are highly associated concentrations of mAb2-Au@PtNPs.

7. Selection of suitable kind of sealer for block surface of mAb2-Au@PtNPs

We chose a suitable kind of sealer for block surface of mAb-Au@PtNPs to reduce non-specific adsorption. A series of sealant (10 % BSA; 10% PEG; 10% Casein; 10% BSA+10% PEG; 10% BSA+10% Casein; 10% PEG+10% Casein; 10% BSA+10% Casein+ 10% PEG) were analyze. In the process of these experiments, 5 μL mAb-MBs were mixture with 94 μL PBS and 6 μL mAb-Au@PtNPs. After incubated 30 min, these mixtures were washed 5 times with PBST buffer. Then these mixtures were incubated with 100 μL 80 μM H_2O_2 for 30 min and following added in 100 μL triangular AgNPRs. After 30 min, mixture was transferred onto a microplate and the intensity of transmitted light was analyzed by the smart phone based NPRP. As shown in Figure S7, the sealer that contained 10% BSA, 10% PEG and 10% casin exhibited the lowest nonspecific adsorption to mAb-MBs. Therefore, in following work, we select this sealer for block surface of mAb-Au@PtNPs.

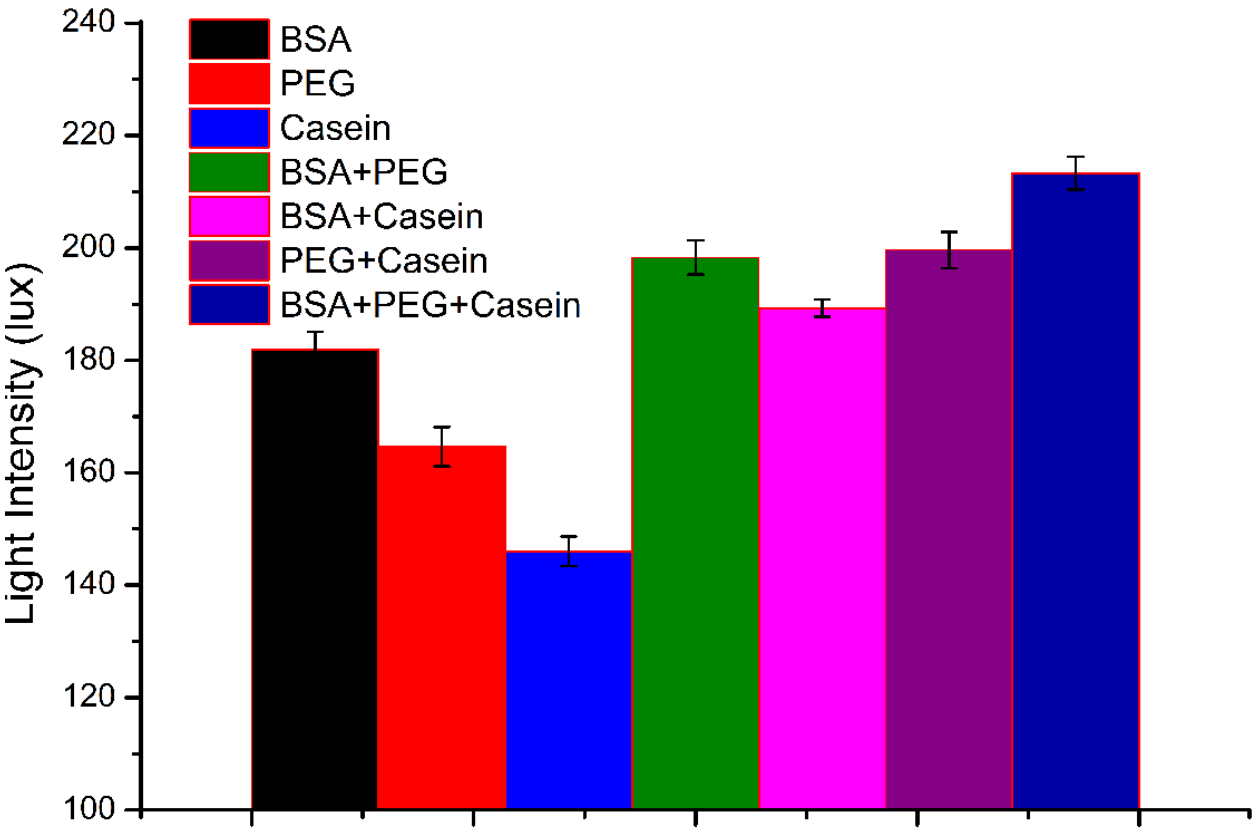

Figure S7. Selection of suitable kind of sealer for block surface of mAb2-Au@PtNPs

8. Optimization of the desired volume of mAb2-Au@PtNPs to use in the plasmonic nanosensors

In this immunoassay, a small quantity of mAb-Au@PtNPs used will decrease detection sensitivity of the plasmonic nanosensors, and even lead to the false negative of detection result. However, larger quantity of mAb-Au@PtNPs probes used in this immunoassay can lead to high nonspecific backgrounds. For optimize the volume of mAb-Au@PtNPs used in plasmonic nanosensors, 0 µL, 2 µL, 4 µL, 6 µL, 8 µL, and 10 µL of mAb-Au@PtNPs were implemented respectively. The volume of MBs probes used in plasmonic nanosensors was 5 µL. The result showed that then volume of used mAb-Au@PtNPs was 4 µL, the difference of measured transmitted light intensity for detects 0 pg/mL of CEA and 50 pg/mL of CEA was the maximum (figure S8). Therefore, volume of mAb-Au@PtNPs used in plasmonic nanosensors was selected as 4 µL.

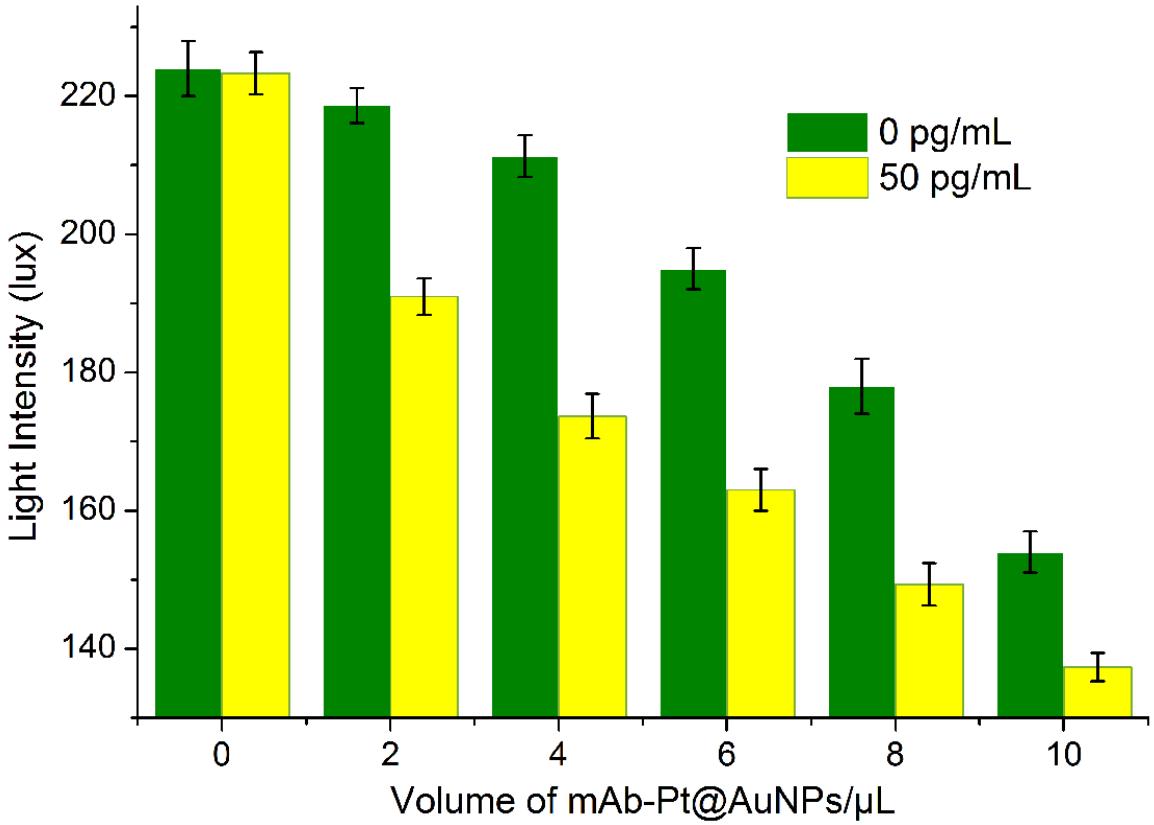

Figure S8. Optimization of the desired volume of mAb2-Au@PtNPs to use in the plasmonic nanosensors

9. Calibration curve of plasmonic nanosensors for detect CEA

The developed smart phone based plasmonic nanosensors were implemented to detect different concentrations of CEA. Along with increasing CEA concentrations the A680 of AgNPRs gradually increased. Furthermore, as CEA concentrations increase, measured A680 increase. Measured A680 was employed to quantitatively measure concentrations of CEA. A good linear correlation (R^2=0.998) between measured A680 and CEA concentration was obtained within the range of 16 pg/mL -512 pg/mL. The LOD of CEA plasmonic nanosensors from A680 of AgNPRs was calculated to be 5.8 pg/mL.

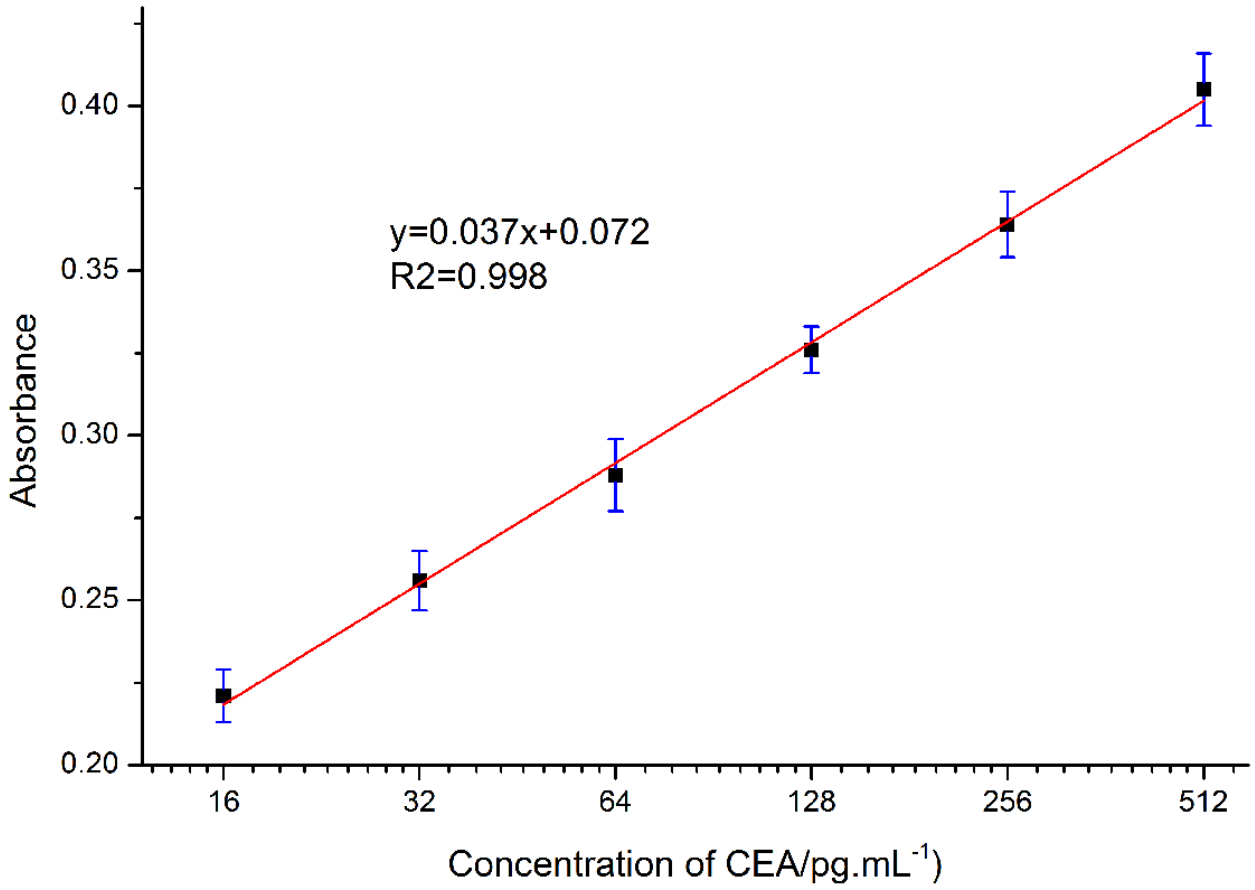

Figure S9. Calibration curve of plasmonic nanosensors for detect CEA. A good linear correlation (R^2=0.998) between measured A680 and CEA concentration was obtained within the range of 16 pg/mL -512 pg/mL. The LOD of CEA plasmonic nanosensors from A680 of AgNPRs was calculated to be 5.8 pg/mL.

10. The specificity of plasmonic nanosensors for detecting CEA

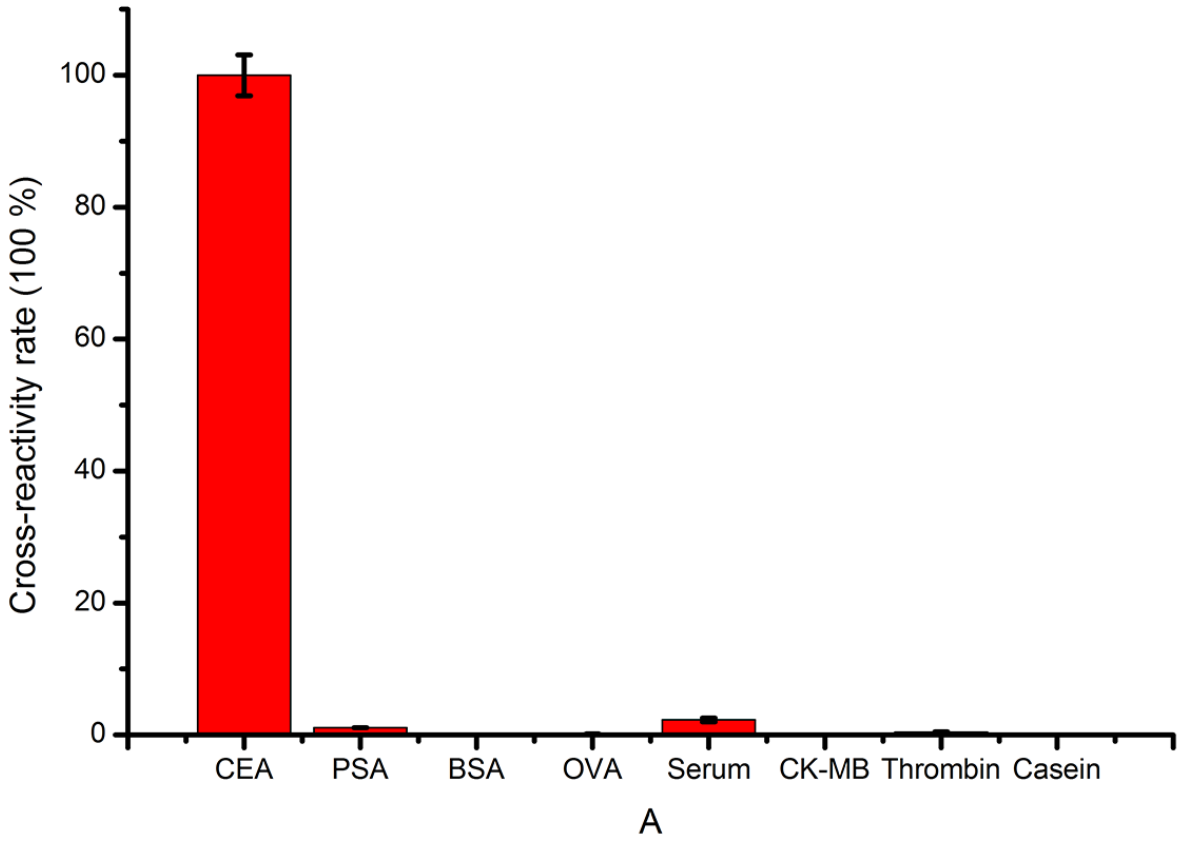

Figure S10. Specificity of plasmonic nanosensors for detecting CEA.

11. Absorbance of AuNPs for detects different concentrations ATP

When ATP concentrations increase, the A525 of AuNPs gradually increases.

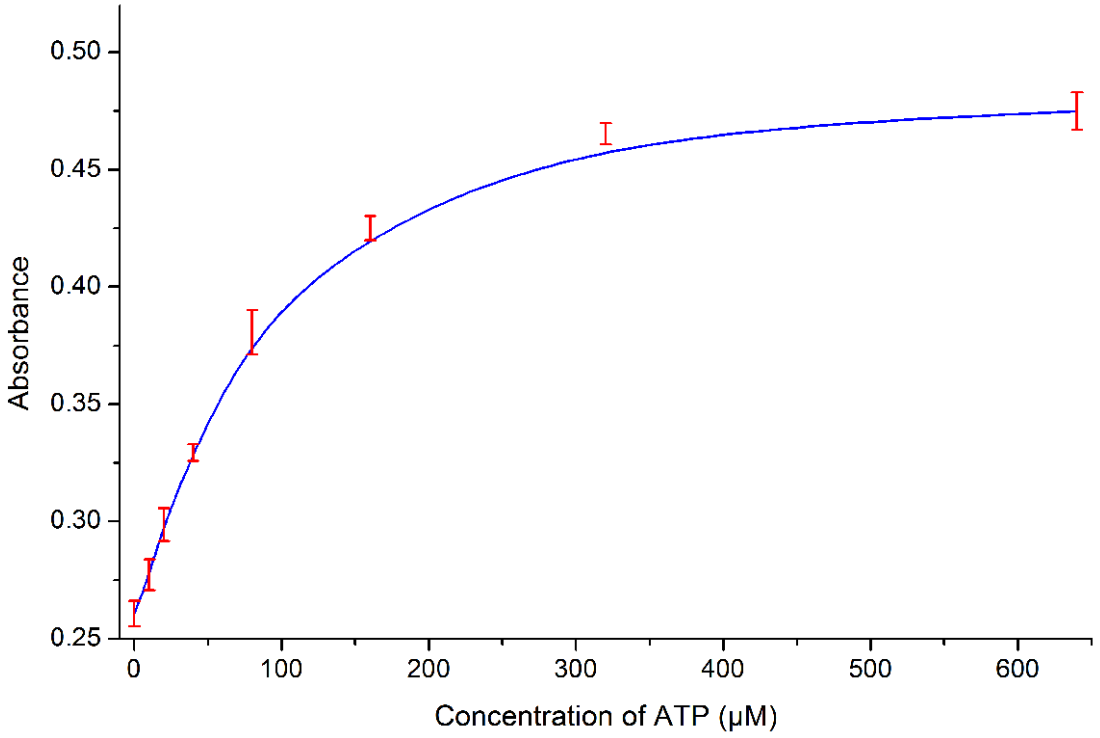

Figure S11. Plasmonic nanosensors for detection of ATP. When ATP concentrations increase, the A525 of AuNPs gradually increases.

12. Calibration curve of plasmonic nanosensors for detect ATP

Measured A525 was employed to quantitatively measure concentrations of ATP. A good linear correlation (R2=0.998) between measured A525 and ATP concentration was obtained within the range of 20 µM - 320 µM. The LOD of ATP plasmonic nanosensors from A525 of AgNPRs was calculated to be 5.6 µM.

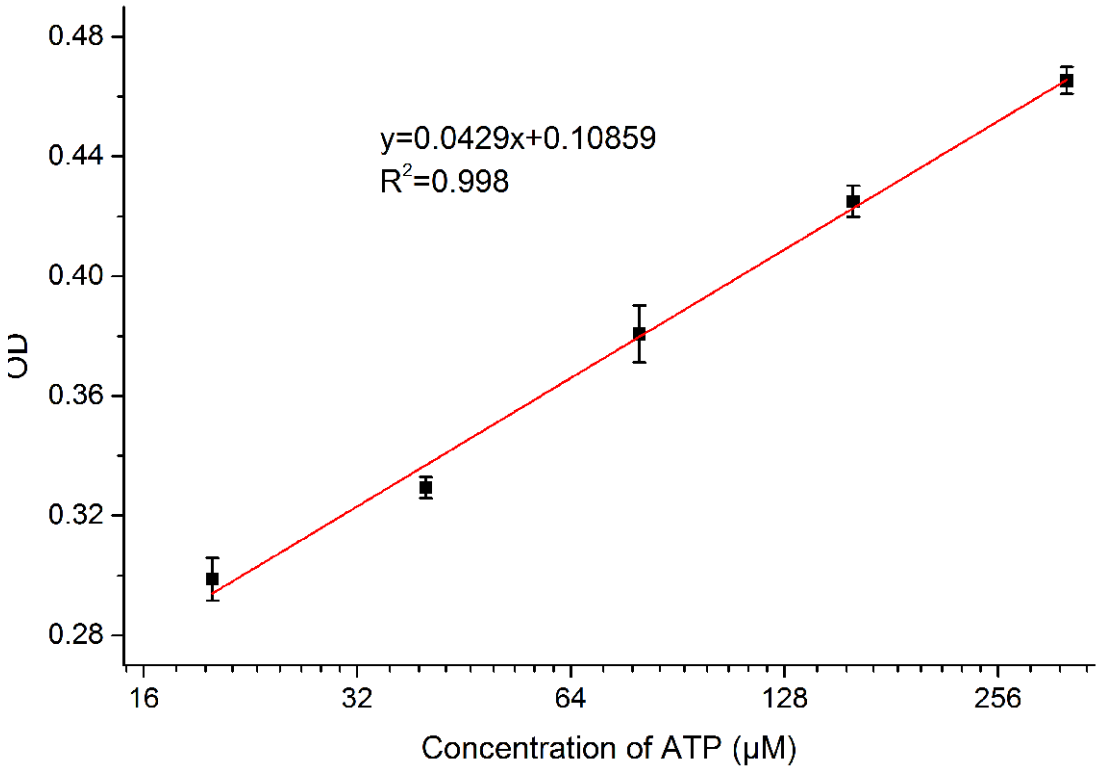

Figure S12. Calibration curve of plasmonic nanosensors for detect ATP.

13. Specificity of plasmonic nanosensors for detection of ATP.

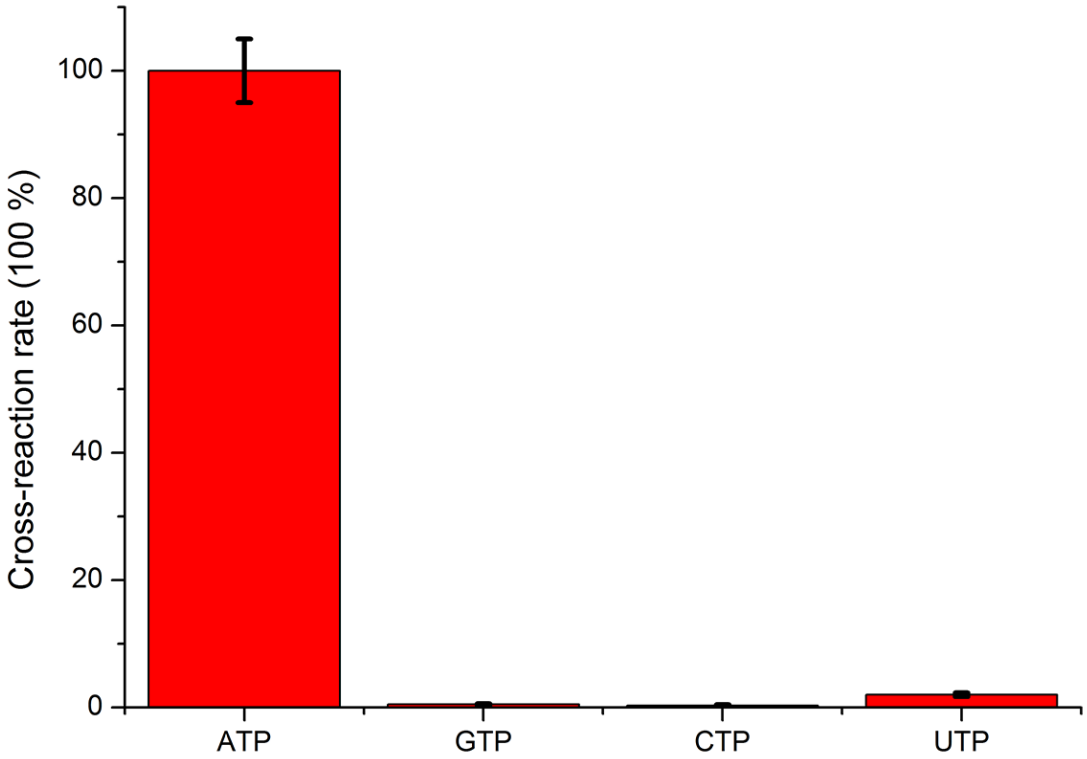

Figure S13. Specificity of plasmonic nanosensors for detection of ATP.

14. Comparison of detect ATP in serum using the smart phone-based PNRP and commercial assay kit

Table S1. Detection of ATP in serum using the smart phone-based PNRP and commercial assay kit

Spiked ATP concentration (μM)	Results from smart phone-based PNRP (μM)	Results from commercial assay kit (μM)
50	68.3±13.5	57.8±5.5
100	122.3±25.6	114.5±13.5
150	181.1±27	142.7±15.2
200	254.6±35.6	213.1±8.4

Table S2. Summary of reported plasmonic nanosensors

	Analyte	Nanosubstrate	The reason	LSPR wavelength	Reference
Gold Nanoparticles aggregation	ATP	Gold Nanoparticle	Salt-induced aggregation	525 nm	[1]
	Pesticides	Gold Nanoparticles	Thiocholine-induced aggregation	525 nm	[2]
	Rabbit antihuman IgG	Gold Nanoparticles	Enzyme-Triggered Click Chemistry	525 nm	[3]
	Pathogens	Gold Nanoparticles	Acetylcholinesterase-induced aggregation	525 nm	[4]
	Influenza Virus Receptor	Gold nanoparticle	Viral hemagglutinin induced aggregation	525 nm	[5]
	peptide	Gold nanoparticle	Peptide -induced aggregation	525 nm	[6]
	Creatinine	Gold nanoparticle	Coordination chemistry induced aggregation	525 nm	[7]
	anti-gp41 IgG	Gold nanoparticle	Copper-mediated click chemistry	525 nm	[8]
	H_2O_2	Gold nanoparticle	Cysteine induced aggregation	525 nm	[9]
	Mercury	Gold nanoparticle	Salt-induced aggregation	525 nm	[10]
	DNA	Gold nanoparticle	L-Cysteine induced aggregation	525 nm	[11]
	Sinefungin	Gold nanoparticle	Antibody induced aggregation	525 nm	[12]
	Anti-HCV mabs	Gold nanoparticle	H_2O_2 mediated aggregation	525 nm	[13]
	gp120	Gold nanoparticle	H_2O_2 mediated aggregation	525 nm	[14]
	Prostate specific antigen	Gold nanoparticle	H_2O_2 mediated aggregation	525 nm	[15]
	Pathogen	Gold nanoparticle	Cysteine induced aggregation	525 nm	[16]
	Amyloid β-peptide	Gold nanoparticle	Cu^{2+}induced aggregation	525 nm	[17]
Nanomaterials morphology change	Glucose	Silver Nanoprism	Etched by H_2O_2 aggregation	680 nm	[18]
	DNA	Silver Nanoprism	etched by H2O2 produced glucose glucoamylase	680 nm	[19]
	hepatitis B surface antigen	Gold nanoparticle	Gold nanoparticle growth	525 nm	[20]
	Small Molecules	Gold Nanoparticles	Target-mediated growth	625 nm	[21]
	Mercury Ions	Gold Nanoparticles	Form gold amalgam		[22]
	Prostate-specific antigen	Gold Nanoparticles	H_2O_2 mediated growth	525 nm	[23]
	Prostate-specific antigen	Gold nanostars	H2O2 mediated growth	600 nm	[24]

References and notes

1. J. Wang, L. Wang, X. Liu, Z. Liang, S. Song, W. Li, G. Li and C. Fan, *Advanced Materials*, 2007, **19**, 3943-3946.
2. D. Liu, W. Chen, J. Wei, X. Li, Z. Wang and X. Jiang, *Analytical chemistry*, 2012, **84**, 4185-4191.
3. Y. Xianyu, Z. Wang and X. Jiang, *ACS nano*, 2014, **8**, 12741-12747.
4. D. Liu, Z. Wang, A. Jin, X. Huang, X. Sun, F. Wang, Q. Yan, S. Ge, N. Xia and G. Niu, *Angewandte Chemie International Edition*, 2013, **52**, 14065-14069.
5. J. Wei, L. Zheng, X. Lv, Y. Bi, W. Chen, W. Zhang, Y. Shi, L. Zhao, X. Sun and F. Wang, *ACS nano*, 2014, **8**, 4600-4607.
6. L. Wei, X. Wang, C. Li, X. Li, Y. Yin and G. Li, *Biosensors and Bioelectronics*, 2015, **71**, 348-352.
7. J. Du, B. Zhu, W. R. Leow, S. Chen, T. C. Sum, X. Peng and X. Chen, *Small*, 2015, **11**, 4104-4110.
8. W. Qu, Y. Liu, D. Liu, Z. Wang and X. Jiang, *Angewandte Chemie*, 2011, **123**, 3504-3507.
9. F. Wang, X. Liu, C.-H. Lu and I. Willner, *ACS nano*, 2013, **7**, 7278-7286.
10. Q. Wei, R. Nagi, K. Sadeghi, S. Feng, E. Yan, S. J. Ki, R. Caire, D. Tseng and A. Ozcan, *ACS nano*, 2014, **8**, 1121-1129.
11. A. Niazov‐Elkan, E. Golub, E. Sharon, D. Balogh and I. Willner, *Small*, 2014, **10**, 2883-2891.
12. Z. Zhen, L.-J. Tang, H. Long and J.-H. Jiang, *Analytical chemistry*, 2012, **84**, 3614-3620.
13. Y. Xianyu, Y. Chen and X. Jiang, *Analytical chemistry*, 2015, **87**, 10688-10692.
14. D. Cecchin, R. de La Rica, R. Bain, M. Finnis, M. Stevens and G. Battaglia, *Nanoscale*, 2014, **6**, 9559-9562.
15. R. De La Rica and M. M. Stevens, *Nature nanotechnology*, 2012, **7**, 821-824.
16. M.-P. N. Bui, S. Ahmed and A. Abbas, *Nano letters*, 2015, **15**, 6239-6246.
17. Y. Zhou, H. Dong, L. Liu and M. Xu, *Small*, 2015, **11**, 2144-2149.
18. Y. Xia, J. Ye, K. Tan, J. Wang and G. Yang, *Analytical chemistry*, 2013, **85**, 6241-6247.
19. X. Yang, Y. Yu and Z. Gao, *ACS nano*, 2014, **8**, 4902-4907.
20. M.-P. Peng, W. Ma and Y.-T. Long, *Analytical chemistry*, 2015.
21. J. H. Soh, Y. Lin, S. Rana, J. Y. Ying and M. M. Stevens, *Analytical chemistry*, 2015, **87**, 7644-7652.
22. Z. Chen, C. Zhang, Q. Gao, G. Wang, L. Tan and Q. Liao, *Analytical chemistry*, 2015, **87**, 10963-10968.
23. D. Liu, J. Yang, H.-F. Wang, Z. Wang, X. Huang, Z. Wang, G. Niu, A. Hight Walker and X. Chen, *Analytical chemistry*, 2014, **86**, 5800-5806.
24. L. Rodríguez-Lorenzo, R. de La Rica, R. A. Álvarez-Puebla, L. M. Liz-Marzán and M. M. Stevens, *Nature materials*, 2012, **11**, 604-607.